

PROSPECT SCALE INTERPRETATION OF HRAM DATA: EULER DEPTH ESTIMATES

DR. ALAN B. REID*

ABSTRACT

Euler deconvolution has been applied to magnetic profile data since 1982 and to gridded data since 1990, most often in regional studies, to delineate structural features and indicate their depth. Prospect scale work has mostly been done on a proprietary basis and is therefore not available in the literature. An example of the methods employed, applied to the Geological Survey of Canada's (GSC) Cypress Hills dataset, is given in this paper. Examination of the spatial power spectrum of the grid identifies three source ensembles at spectral slope depths of 500 m, 3 km and 12 km. The effects of the 3 km ensemble are enhanced relative to the others by spectral shaping in the wavenumber domain. Euler deconvolution is applied to this residual, using a moving 4 x 4 km window. Statistical considerations indicate a structural index of 1.0 is the most useful. Zooming in on the solution display and viewing in perspective allows detailed examination of an example feature, two linears (probably faults) intersecting in plan, but at different depths.

INTRODUCTION

Euler deconvolution can be applied to either profiled or gridded magnetic survey data to estimate location and depth of magnetic features such as dipoles (small isolated bodies), monopoles (pipe intrusions), sheets (dykes or shale beds) or blocks (contacts or faults). Euler deconvolution has found wide application to regional studies and depth to basement work, much of it proprietary and unpublished. Published study areas include the Witwatersrand Basin (Durrheim, 1983; Corner and Wilsher, 1989), the Ashanti Gold Belt of Ghana (Beasley and Golden, 1993), Wales (McDonald et al., 1992), and the Sudbury structure (Hearst and Morris, 1993). Provided care is exercised, it can also be applied to locate and map intrasedimentary features.

THEORY AND METHOD

Euler's homogeneity relation may be stated succinctly in the form

$$(x-x_0) \partial T / \partial x + (y-y_0) \partial T / \partial y + (z-z_0) \partial T / \partial z = N(B-T),$$

where (x_0, y_0, z_0) is the position of a source whose total field T is detected at (x, y, z) . The total field has a regional or background value B . N is the degree of homogeneity, interpreted physically as the fall-off rate with distance and geophysically as a structural index (SI). Thompson (1982) developed the profile technique ($\partial T / \partial y = 0$) quite fully, named it EULDPH, and suggested that SIs between 0.5 and 3 were useful on pole reduced magnetic data. Thompson's contact model (SI 0.5) required some empirically based corrections to obtain depth. Reid et al. (1990) followed up a suggestion in Thompson's paper and developed the equivalent method operating on gridded magnetic data. They introduced the concept of the zero SI for contacts, discovered that pole reduction was unnecessary and that no assumptions need be made about the absence of remanence. They coined the term "Euler deconvolution" by analogy with "Werner deconvolution".

As preparation, the total field gradients must either be measured or calculated (typically using Fourier methods). In either case the profile or grid is sampled using a moving window whose selected size is large enough to contain significant field curvature from sources of likely interest, but small enough to minimize effects from adjacent sources. For each profile sample point or grid point in the window, one equation may be written, so that the window provides an overdetermined equation set which may be solved by least squares methods for estimated values of x_0, y_0, z_0 and B and their uncertainties. Simple methods assume that adjacent sampling points are independent measurements. Since this is seldom true, the uncertainties will often be underestimates. It is at present necessary to assume an SI value because direct solution poses an unstable non-linear problem. Where the main targets are faults of small throw interrupting thin shale beds, the actual signal is the superposition of two sheet edge anomalies and an SI value as high as 2 may be appropriate. Isolated sheet edges require an SI of unity and faults moving blocks of significant thickness require SI values approaching zero.

Presented at CSEG HRAM Forum, Calgary, 18th November 1997.

*GETECH, c/o School of Earth Sciences, Leeds University, Leeds, LS2 9JT; now at: Reid Geophysics, 49 Carr Bridge Dr., Leeds LS16 7LB, UK, E-mail: alan@reidgeophys.freeserve.co.uk

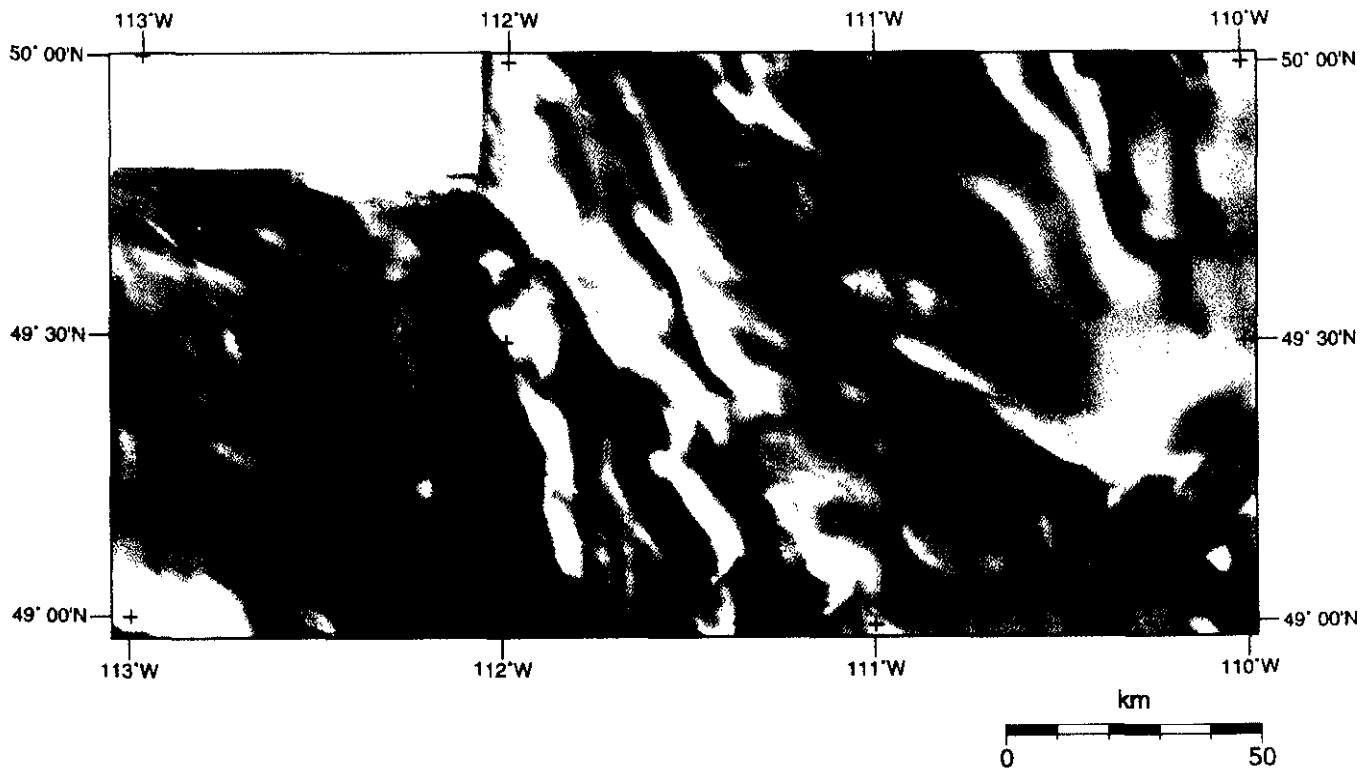


Fig. 1. Aeromagnetic data from Cypress Hills, Alberta, provided by the Geological Survey of Canada. Some magnetic effects from the town of Lethbridge, Alberta can be seen at about 49°40'N, 112°50'W.

PROSPECT-LEVEL STUDIES

Physically meaningful residuals

Much of the prospect-scale work is petroleum exploration-related and unpublished because the data are still commercially valuable. The main difficulty with prospect-scale Euler work is that HRAM data have been optimized to examine intrasedimentary features, whereas the field gradients will normally still be dominated by basement-derived gradients. In principle this could be dealt with by additionally solving for background gradient values, but the process becomes unstable in practice. Prospect scale work is more effective on residual data where basement-related gradients have been removed, by some form of high-pass filtering, such as matched filtering or pseudo-depth slicing. Any such high-pass filtering should be conducted in such a way as to preserve the potential field nature of the data.

The Cypress Hills data set – A demonstration study to investigate prospect scale magnetic features was carried out on the GSC's Cypress Hills data set for the HRAM conference. The original data were received in the form of a grid at a spacing of 400 m (Fig. 1).

Optimum log power spectrum and ensemble enhancement – The power spectrum of the grid, averaged over azimuth (Spector & Grant, 1970) was produced, employing a triangular spectral window on the grid for optimal power esti-

mation (Blackman & Tukey, 1958). The result is shown in Figure 2. It is clear that there are three source ensembles present, with spectral depths of 500 m, 3 km and 10 km, (if the ensemble magnetizations are assumed to be spatially uncorrelated – Spector & Grant, 1970). The power spectrum was used to design a spectral tailoring scheme to generate three grids with each grid focussing on one of the three ensemble depths.

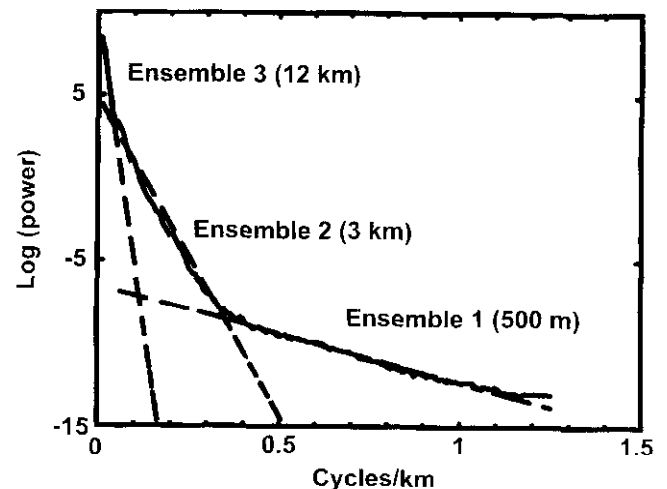


Fig. 2. Optimally estimated log power spectrum of the Cypress Hills magnetic total field of Figure 1, showing source ensembles and their characteristic slope depths.

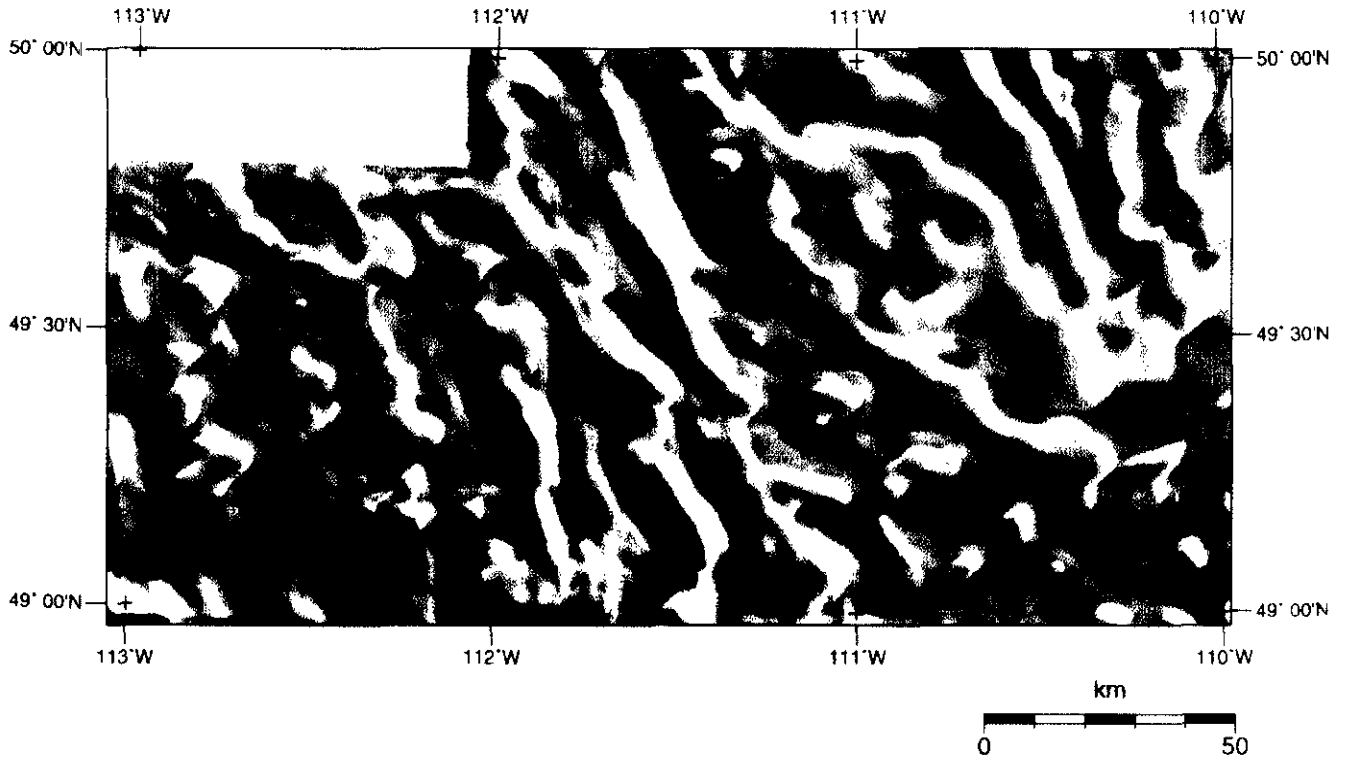


Fig. 3. Cypress Hills aeromagnetic data after preferential enhancement of ensemble 2 with a slope depth of 3 km. Shallower and deeper source effects have been attenuated. Illuminated from the NE.

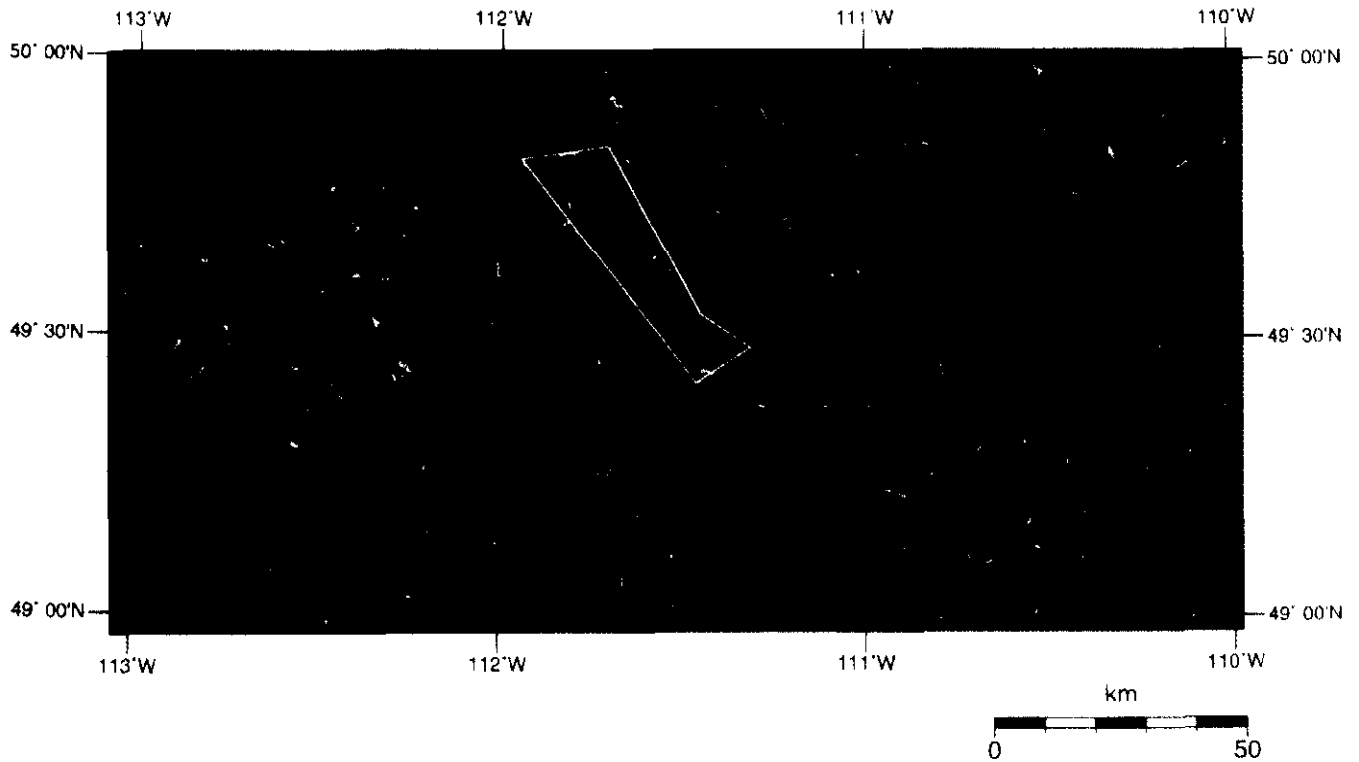


Fig. 4. Euler deconvolution of ensemble 2. Structural index 1.0, window size 4 km. Depth colours range from red (2 km) to deep blue (4 km). Zoom area outlined in white.

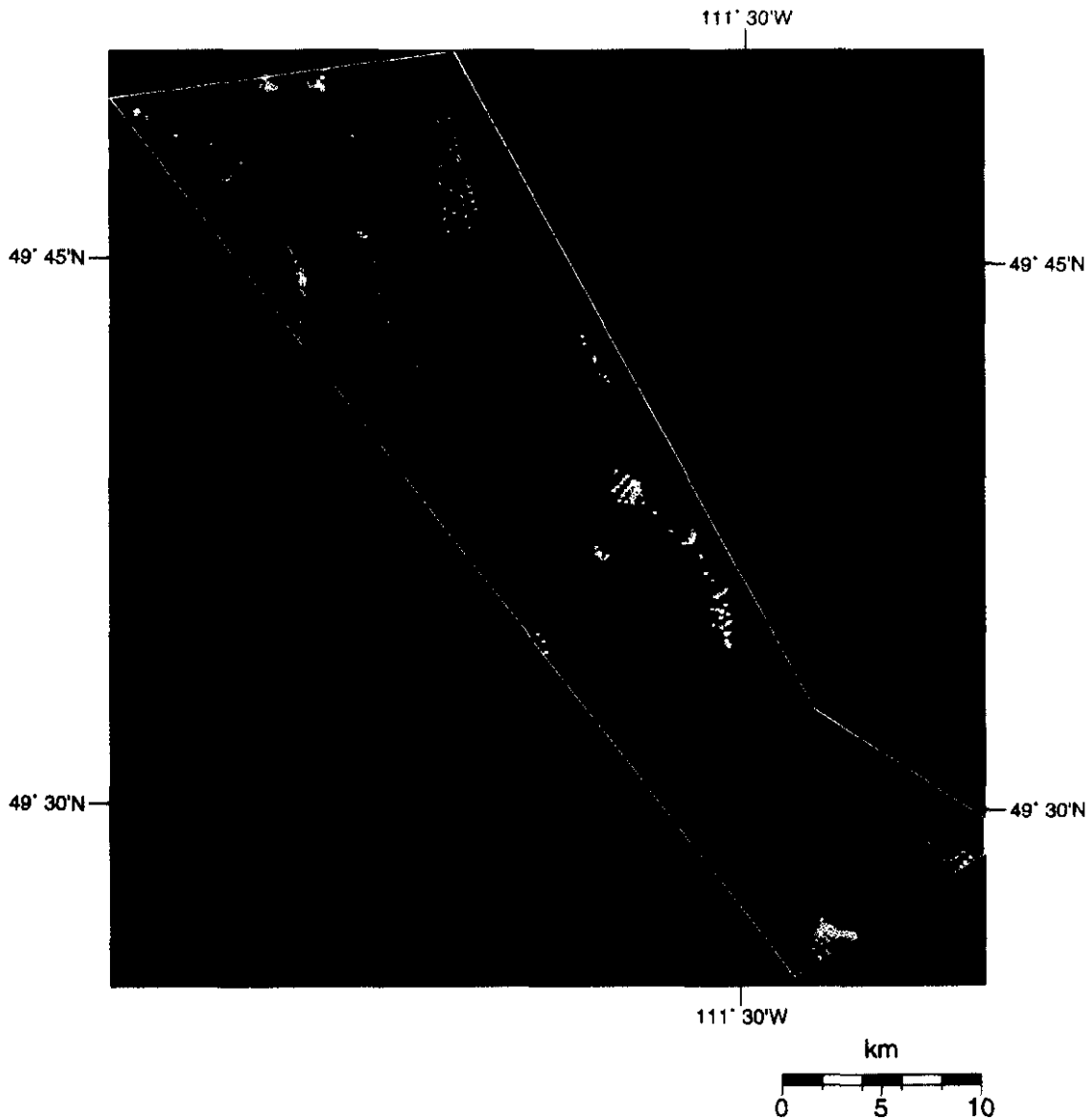


Fig. 5. Enlargement of the white outlined area of Figure 4.

Wavenumber-selective attenuation of the original grid was used to fit each of the three power spectrum slopes. This process goes by many names, including spectral tailoring, swing-tail filtering (Cordell, 1985), pseudo-depth slicing and ensemble enhancement. The latter term has been adopted here.

The shallowest ensemble grid (slope depth 500 m – not shown here) is dominated by shallow structures, the Eocene Lethbridge Dikes and mislevelling artifacts and has not been employed further. The deepest ensemble grid (slope depth 12 km – not shown here) was regarded as favouring deep geological structure of only indirect interest for petroleum prospecting. The remaining ensemble map or pseudo-depth slice (slope depth 3 km) is presented as a shaded, coloured image in Figure 3. As may be seen, the image shows some roughly equidimensional features, others with NNW-SSE strike and a more subtle NW-SE set. The regional slope

across the area has disappeared. Some short-wavelength features (possibly of cultural origin) have disappeared. Intermediate wavelength features are enhanced, but a good range of wavelengths still exists.

Euler deconvolution of residual grid – This ensemble residual grid with a slope depth of 3 km was subjected to Euler deconvolution using a 4 km x 4 km (10 x 10 grid cell) window and structural indices of 0.0, 0.5 and 1.0, including curvature discrimination (Fairhead et al., 1994). A larger window would reduce lateral resolution. A smaller window would yield poor results given the ensemble depth (Reid et al., 1990). Statistical examination of the resulting solutions showed that the SI 1.0 data (mean depth 3.2 ± 0.8 km) gave the best fit to the ensemble average depth (the other SIs gave shallower mean depths, making them inconsistent with the ensemble spectral slope – see Table 1). This suggests that the

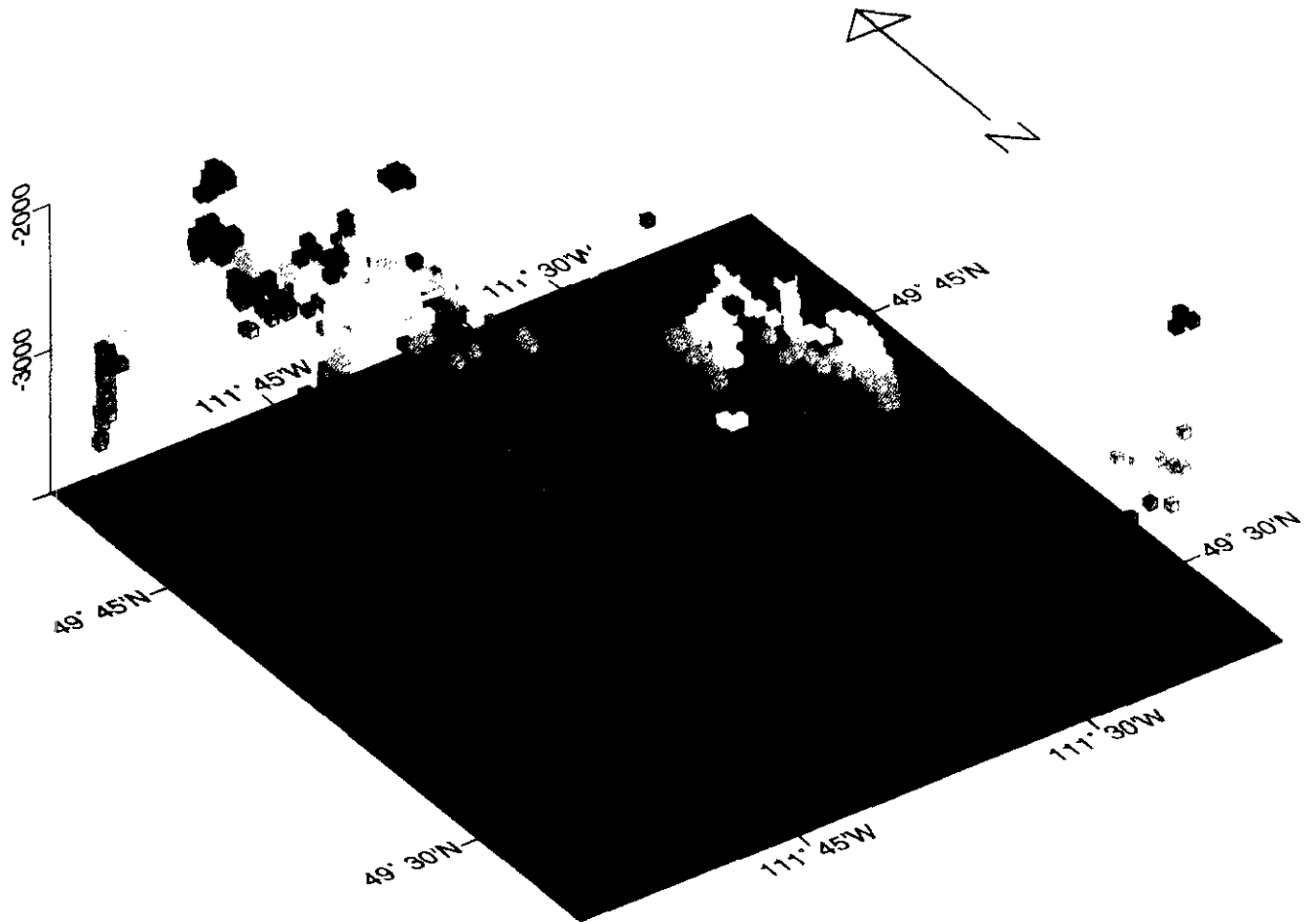


Fig. 6. Perspective view of the zoomed area. Looking downward, towards the NE. Depth range shown is 2000 - 4000 m.

majority of magnetic sources should be regarded as being thin (SI 1.0 is characteristic of thin sheet edges). The least squares equation solution permits estimation of uncertainty of depth (ΔZ) and horizontal location (ΔH). Normalization of both of these to the estimated depth (Z) produces goodness of fit parameters approximately independent of depth. The distributions of $\Delta Z/Z$ and $\Delta H/Z$ were also examined and optimum selection values chosen. The statistics are summarized in Table 1. Selection is necessary because the process produces some meaningless high-uncertainty results which are best removed (Reid et al., 1990).

Table 1. Euler solution depth statistics using a structural index (SI) between 0.0 and 1.0. Results have been confined to the depth (Z) range 2 - 4 km and depth-normalized maximum depth ($\Delta Z/Z$) and location ($\Delta H/Z$) uncertainties as tabulated. Uncertainties in X, Y and Z are ΔX , ΔY and ΔZ respectively. Horizontal uncertainties were combined using $(\Delta H)^2 = (\Delta X)^2 + (\Delta Y)^2$

| SI | Mean depth (km) | $\Delta Z/Z$ (%) | $\Delta H/Z$ (%) |
|-----|-----------------|------------------|------------------|
| 1.0 | 3.2 ± 0.8 | 6 | 12 |
| 0.5 | 2.4 ± 0.7 | 5 | 15 |
| 0.0 | 1.6 ± 0.5 | 5 | 20 |

In a full structural analysis, it would be necessary to consider a wide range of structural indices and examine the choice of SI, feature by feature. For the sake of illustration, the discussion here only looks at one index (1.0), which is in any case favoured for reasons discussed above. The Euler deconvolution results are shown in Figure 4. The deconvolution has identified features with depths between 2000 m (red) and 4000 m (deep blue). They show the locations and strikes of features in general are similar to the more obvious features in Figure 3. A full interpretation of everything in the figure is beyond the scope of this paper, which is merely intended to be illustrative. One particular area is expanded and examined. That area is outlined by the white zoom polygon in Figure 4 and reveals two features, one striking NW-SE and the other striking NNW-SSE with some disruption along strike. The feature is shown enlarged in Figure 5. It is apparent from this figure that the NW-SE feature passes beneath its partner. Additional features seen are the "strings of pearls". Such "pearls" are a widely reported artifact of the method. They were until recently considered to be of no use whatsoever but Kuttikul et al. (1995) have recently shown that they are dip sensitive, the first indication that dip can be

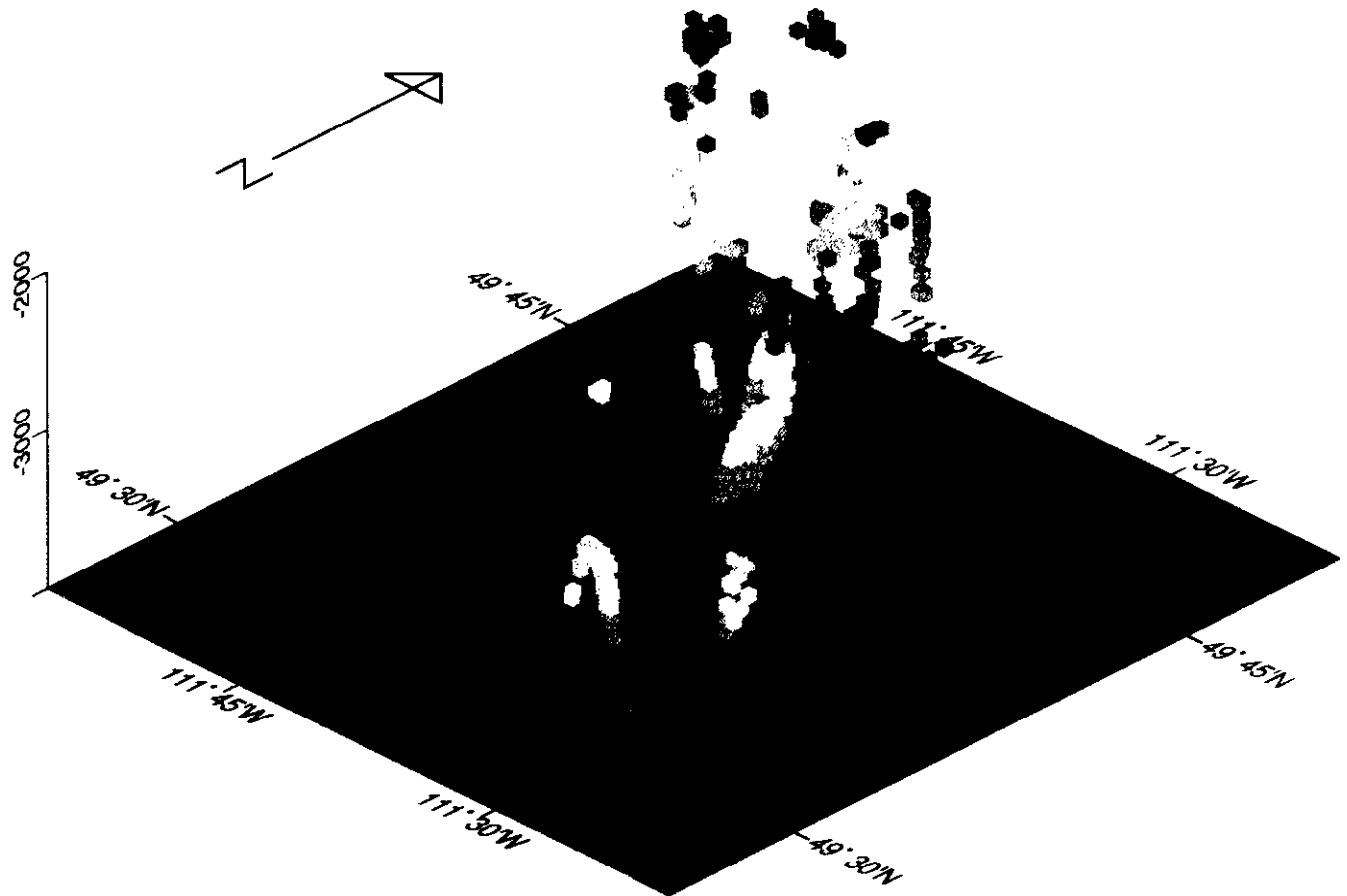


Fig. 7. Perspective view of the zoomed area. Looking downward, towards the NW. Depth range shown is 2000 - 4000 m.

estimated using Euler deconvolution. The detailed features may further be examined in perspective. Figure 6 shows the zoomed area, looking downward, towards the NE, whereas Figure 7 shows the same area viewed looking towards the NW. The NW viewing direction is more or less along strike and clearly shows the NW-SE feature passing beneath the NNW-SSE one. The data as seen looking in this direction could have been interpreted as a single dipping sheet, were it not for the knowledge provided by Figures 5 and 6. With that insight, the NW-SE feature can again be seen passing beneath its companion.

A full interpretation would employ available geological knowledge of the area to assist in identifying and modeling the features discussed, as well as others displayed by the deconvolution. While this is beyond the scope of this contribution, it is interesting to surmise that both linears may be fault edges disrupting local magnetically active lithologies, such as shale bands. The main purpose of the paper is to illustrate that prospect-scale structural detail can be displayed and understood using Euler deconvolution on an appropriate data set when the results are viewed using the graphical display power available in any modern workstation.

CONCLUSION

It is concluded that prospect scale application of grid Euler deconvolution is possible. The best results are obtained by applying the method to physically meaningful residual grids, rather than to total field observations.

ACKNOWLEDGMENTS

The Geological Survey of Canada gave permission to use the Cypress Hills data for demonstration purposes. I also acknowledge the support of Robertson Research during the original development of grid Euler deconvolution and the practical and financial support of the management and staff of GETECH during the redevelopment of the current software package and during the preparation of this paper. In particular, I am indebted to Alison Hollins, Paul Black and Robert Daniels for their assistance in preparing and modifying the figures.

REFERENCES

- Beasley, C.W., and Golden, H.C., 1993. Application of Euler Deconvolution to Magnetics Data from the Ashanti Belt, Southern Ghana: 63rd Ann. Internat. Mtg. Soc. Expl. Geophys., Expanded Abstracts, 417-420.

- Blackman, R.B., and Tukey, J.W., 1958, The measurement of power spectra from the point of view of communications engineering: Dover.
- Cordell, L., 1985, A stripping filter for potential field data: 55th Ann. Internat. Mtg., Soc. Expl. Geophys., Expanded Abstracts, 217-218.
- Corner, B., and Wilsher, W.A., 1989, Structure of the Witwatersrand Basin derived from interpretation of aeromagnetic and gravity data: in Garland, G.D., Ed., Proceedings of Exploration '87: Third Decennial international conference on geophysical and geochemical exploration for minerals and groundwater. Ontario Geological Survey, Special Volume 3, 532-546.
- Durrheim, R.J., 1983, Regional-residual separation and automatic interpretation of aeromagnetic data: M.Sc. thesis, Univ. of Pretoria.
- Fairhead, J.D., Bennett, K.J., Gordon, R.H., and Huang, D., 1994, Euler: Beyond the "Black Box": 64th Ann. Internat. Mtg., Soc. Expl. Geophys., Expanded Abstracts, 422-424.
- Hearst, R.B., and Morris, W.A., 1993, Interpretation of the Sudbury Structure through Euler Deconvolution: 63rd Ann. Internat. Mtg., Soc. Expl. Geophys., Expanded Abstracts, 421-424.
- Kuttikul, P., Barritt, S., and Hanssen, R., 1995, Maximization of geological information in 3D Euler deconvolution: 57th Ann. Conf. & Tech. Exhib., Eur. Assoc. Expl. Geophys., Extended Abstract D031.
- McDonald, A.J.W., Fletcher, C.J.N., Carruthers, R.M., Wilson, D., and Evans, R.B., 1992, Interpretation of the regional gravity and magnetic surveys of Wales, using shaded relief and Euler deconvolution techniques: Geol. Mag., **129**, 523-531.
- Reid, A.B., Allsop, J.M., Granser, H., Millett, A.J., and Somerton, I.W., 1990, Magnetic interpretation in three dimensions using Euler deconvolution: Geophysics, **55**, 80-91.
- Spector, A., and Grant, F.S., 1970, Statistical models for interpreting aeromagnetic data: Geophysics, **35**, 293-302.
- Thompson, D.T., 1982, EULDPH – a new technique for making computer-assisted depth estimates from magnetic data: Geophysics, **47**, 31-37.